The USP1 Inhibitor KSQ-4279 Overcomes PARP Inhibitor Resistance in Homologous Recombination–Deficient Tumors

Louise Cadzow[1], Jehrod Brenneman[1], Erica Tobin[1], Pamela Sullivan[1], Sumeet Nayak[1], Janid A. Ali[1], Sol Shenker[1], Jim Griffith[1], Michael McGuire[1], Paula Grasberger[1], Yuji Mishina[1], Morgan Murray[1], Anne E. Dodson[1], Hugh Gannon[1], Elsa Krall[1], Jeff Hixon[1], Edmond Chipumuro[1], Kerstin Sinkevicius[1], Prafulla C. Gokhale[2], Suthakar Ganapathy[2], Ursula A. Matulonis[3], Joyce F. Liu[3], Andrew Olaharski[1], Dipen Sangurdekar[1], Hanlan Liu[1], Jeremy Wilt[1], Michael Schlabach[1], Frank Stegmeier[1], and Andrew A. Wylie[1]

ABSTRACT

Defects in DNA repair pathways play a pivotal role in tumor evolution and resistance to therapy. At the same time, they create vulnerabilities that render tumors dependent on the remaining DNA repair processes. This phenomenon is exemplified by the clinical activity of PARP inhibitors in tumors with homologous recombination (HR) repair defects, such as tumors with inactivating mutations in *BRCA1* or *BRCA2*. However, the development of resistance to PARP inhibitors in BRCA-mutant tumors represents a high unmet clinical need. In this study, we identified deubiquitinase ubiquitin-specific peptidase-1 (USP1) as a critical dependency in tumors with *BRCA* mutations or other forms of HR deficiency and developed KSQ-4279, the first potent and selective USP1 inhibitor to enter clinical testing. The combination of KSQ-4279 with a PARP inhibitor was well tolerated and induced durable tumor regression across several patient-derived PARP-resistant models. These findings indicate that USP1 inhibitors represent a promising therapeutic strategy for overcoming PARP inhibitor resistance in patients with BRCA-mutant/HR-deficient tumors and support continued testing in clinical trials.

Significance: KSQ-4279 is a potent and selective inhibitor of USP1 that induces regression of PARP inhibitor–resistant tumors when dosed in combination with PARP inhibitors, addressing an unmet clinical need for BRCA-mutant tumors.

Introduction

Genomic instability is a hallmark of many cancers and often results from defects in DNA damage response (DDR) pathways (1, 2). Although these defects help drive tumor evolution through the accumulation of genetic alterations, they also leave tumors critically dependent on the remaining functional DDR pathways (3). This presents an opportunity for therapeutic intervention through synthetic lethality, exemplified by the success of PARP inhibitors in treating tumors with *BRCA1* or *BRCA2* mutations. Inactivation of *BRCA1/2* affects the cell's ability to perform critical genome maintenance roles, such as maintaining replication fork stability and promoting double-strand DNA break (DSB) repair through the homologous recombination (HR) pathway (4–7). This inactivation not only promotes tumor evolution but also creates a critical dependency on other DDR pathways, such as the single-strand break repair pathway, which is exploited by PARP inhibitors (8). However, it is important to note that not all patients with HR pathway defects respond to PARP inhibitors, and those that do benefit often develop resistance.

Understanding how different DDR pathway defects create specific vulnerabilities that can be exploited therapeutically is confounded by the complexity and functional redundancy of DNA repair processes. One approach to decipher such dependencies is to use CRISPR screens to systematically test the function of all genes in the genome to identify those that are selectively lethal in tumors with specific DNA repair defects. The success of this approach is exemplified by the discovery that tumors with high levels of microsatellite instability, due to defects in the DNA mismatch repair pathway, are selectively dependent on WRN helicase (9).

To develop novel first-in-class treatments that exploit vulnerabilities in tumor cells, we first performed a genome-wide CRISPR screen across >500 cancer cell lines to identify which targets to pursue. These screens revealed that ovarian and breast cancer cell lines, lineages known to harbor defects in HR (10–12), are often dependent on the activity of the deubiquitinase (DUB), USP1, and its heterodimerization partner, USP1-associated factor 1 (UAF1). USP1 has a well-established role in regulating the Fanconi anemia (FA) complex and translesion synthesis (TLS), both of which interface with the HR pathway (13, 14)

To determine the therapeutic potential of targeting USP1 in HR-defective tumors, we undertook a drug discovery campaign to develop a potent, selective inhibitor of USP1 with the necessary drug-like properties to enable clinical testing. KSQ-4279 is efficacious as a single agent in HR-defective tumor models, with mechanism of action studies indicating that KSQ-4279 sensitivity is associated with the accumulation of single-strand DNA (ssDNA) gaps, replication fork instability, and cell death. To gain insight into which DDR pathway(s) influence the sensitivity of cells to KSQ-4279, CRISPR

[1]KSQ Therapeutics, Lexington, Massachusetts. [2]Belfer Center for Applied Cancer Science, Dana-Farber Cancer Institute, Boston, Massachusetts. [3]Dana Farber Cancer Institute, Boston, Massachusetts.

Corresponding Author: Andrew A. Wylie, KSQ Therapeutics, 4 Maguire Road, Lexington, MA 02421. E-mail: awylie@ksqtx.com

Cancer Res 2024;84:3419–34

doi: 10.1158/0008-5472.CAN-24-0293

screens were performed in *BRCA1*-mutant cells. The results of the screen revealed that the loss of genes involved in ubiquitinating PCNA reduced the sensitivity of cells to KSQ-4279, whereas several members of the base-excision repair (BER) pathway, including PARP1, sensitized cells to KSQ-4279. PARP inhibitors are known to be active in tumors with HR defects, and we show that KSQ-4279 synergizes with PARP inhibitors when dosed in combination. The development of resistance to PARP inhibitors in patients with BRCA-mutant tumors is often correlated with the restoration of the HR pathway and has become a high unmet clinical need. Using patient-derived models that reflected this PARP resistance setting, our studies revealed that the resistance to PARP inhibitors could be overcome by dosing KSQ-4279 in combination with a PARP inhibitor, leading to durable tumor regressions. This data supports the current clinical testing of KSQ-4279 in combination with PARP inhibitors.

Materials and Methods

Compounds

KSQ-4279 was discovered and manufactured by KSQ Therapeutics, Inc. For *in vitro* studies, all drug treatments were performed using 10 mmol/L DMSO stock solutions at a final concentration of 0.1% DMSO or lower. For animal studies, all compounds were dosed once daily per oral via gavage at a dose volume of 10 mL/kg. KSQ-4279 was formulated as a 1:1 gentisic acid cocrystal to improve *in vivo* exposure, prepared as a suspension in 0.5% weight volume (hydroxypropyl)methyl cellulose/0.1% volume/volume (v/v) Tween 80 in sterile deionized water and dosed at a final dose range of 10 to 300 mg/kg. Olaparib (developed by AstraZeneca and purchased from MedKoo Biosciences, cat. #200422) was formulated in 10% v/v DMSO in 10% weight volume (2-hydroxypropyl)-β-cyclodextrin in sterile deionized water and dosed at 50 or 100 mg/kg. AZD5305 (developed by AstraZeneca and purchased from MedChemExpress, cat. #HY-132167) was formulated in 10% DMSO/40% polyethylene glycol 400/5% Tween 80 in 0.9% NaCl and dosed at 10 mg/kg.

Cancer cell lines and culture

Human parental cell lines were sourced from ATCC, DSMZ, JCRB, ECACC, and BioIVT. All cell lines were maintained as monolayers in a vendor-recommended medium, as listed in Supplementary Table S1. Cells were maintained at 37°C in an incubator supplemented with 5% carbon dioxide. All cell lines were confirmed to be *Mycoplasma* negative using the BIOWING Applied Biotechnology kit (cat. # BPM50) or the Sigma Lookout Mycoplasma Testing Kit (cat. #MP0035) and authenticated using short tandem repeat profiling.

Generation of KO and overexpression cell lines

CAOV3 cells with *RAD18* KO were generated by Cas9 ribonucleotide co-nucleofection with sgRNA specifically targeting *RAD18* (sgTTACCAGTTCATCTAATATG) using a Lonza 4D-Nucleofector and SE Solution, Pulse Code CA-137. Cells were cultured for 4 days prior to confirmation of target KO by immunoblotting. Overexpression cell lines were generated by cloning cDNA for *PCNA* wild-type, $PCNA^{K164R}$ mutant, *FANCD2* wild-type, or $FANCD2^{K561R}$ mutant into a pLenti6 plasmid (Invitrogen) modified to contain a U6 promoter. Lenti-X 293T cells were transfected with standard viral packaging vectors using TransIT transfection reagent (Mirus Bio). Viral supernatant was filtered using 0.45-μm polyvinylidene difluoride filters (Millipore Sigma). CAOV3 cells were transduced with virus and selected with 2 μg/mL puromycin.

In vitro CRISPR screens

To identify novel targets, pooled genome-wide CRISPR screens with seven sgRNAs per gene were performed across >500 cancer cell lines, following previously published methods (15). Similarly, a DDR-enriched CRISPR library targeting 1,500 genes and containing 20 guides per gene was screened in UWB1.289 cells in the presence of drug treatment in which following the antibiotic selection step, media was removed and replaced with fresh media containing DMSO or 300 nmol/L KSQ-4279. Cells were then cultured in the presence of the drug for 14 days before being harvested for genomic DNA isolation.

Biochemical assays reagents and buffers

All chemicals were of reagent grade. Buffers were made with deionized distilled H_2O. Enzyme reaction buffer: 50 mmol/L HEPES (pH 7.8), 0.5 mmol/L EDTA, 0.01% BSA, 1 mmol/L dithiothreitol and 0.01% Tween 20. Biochemical studies were carried out on purified USP1/UAF1 complex, cloned, and coexpressed in SF1 insect cells according to published protocols (16, 17), with an initial Ni Affinity column to capture His-Tagged USP1 and modified by including a secondary anti-FLAG affinity column to capture FLAG-tagged UAF1. The two-step affinity column procedure yielded pure, active USP1/UAF1 complex, herein referred to as Usp1. The fluorescent enzyme substrate ubiquitin–rhodamine (Ub-Rho) was purchased from R&D Systems (catalog #U-555) and made into a 10 mmol/L stock solution in DMSO. KSQ-4279 was prepared in a 10 mmol/L DMSO stock inhibitor solution.

Enzyme activity and inhibition studies

USP1 activity and its inhibition by KSQ-4279 were determined by monitoring Ub-Rho hydrolysis in a kinetic format (18). In the absence of an inhibitor, USP1 hydrolyzes Ub-Rho, resulting in the release of free Rho and a concomitant increase in fluorescence (19). Assays were carried out in Opti 384F flat black bottom microtiter plates, read in a paradigm plate reader, with excitation and emission wavelengths set to 480 and 540 nm, respectively, and the fluorescence signal was converted to concentrations of free rhodamine produced via a rhodamine calibration curve.

Mode of inhibition studies

The mode of inhibition was studied by determining the impact of KSQ-4279 on the K_m and V_{max} of USP1. Briefly, KSQ -4279 was serially diluted threefold in DMSO and 0.1 μL dispensed into a microtiter plate using an Echo Dispenser (Beckman Coulter). Next, 10 μL of a 2× stock solution of Usp1 was added, and the resulting enzyme inhibitor mixture was incubated for 30 minutes at room temperature. The enzymatic reaction was initiated by the addition of 10 μL of Ub-Rho, yielding a final reaction volume of 20 μL. The final concentrations of Usp1 were 12.5 pmol/L, with KSQ-4279 ranging from 100 to 0.78 nmol/L and Ub-Rho substrate varied from 6,000 to 46.8 nmol/L. The reaction was monitored in a kinetic format, and the initial rates were determined.

Reversibility of KSQ-4279 studies

To assess the reversibility of KSQ-4279, dissociation k_{off} experiments were performed using the jump dilution method. USP1-KSQ-4279 and USP1-KSQ-4279-Ub-Rho substrate complexes were performed by incubating 50 nmol/L KSQ-4279 with 2.5-

nmol/L USP1 ± 5,000-nmol/L Ub-Rhodamine substrate for 30 minutes at room temperature. This was "jump diluted" 300-fold by diluting 1 μL into 300 μL of 1,500-nmol/L Ub-Rho substrate solution and determining the recovery of enzymatic activity in a continuous kinetic manner. In concert, three control reactions were run: (i) a zero inhibitor experiment to measure the uninhibited rate by diluting 2.5-nmol/L Usp1 300 fold directly into 1,500-nmol/L substrate in the absence of inhibitor, (ii) a 100% inhibited control reaction by diluting 2.5-nmol/L Usp1 300 fold into 1,500-nmol/L Ub-Rho substrate and 50-nmol/L KSQ-4279, and (iii) a no pre-incubation inhibitor control whereby 2.5-nmol/L Usp1 and 50-nmol/L KSQ-4279 with no preincubation was diluted 300-fold into 1,500-nmol/L substrate.

Cryo-EM sample preparation

One milligram of UAF1/USP1 and 170.4 μg Ub-PA were combined as follows: glycerol and Ub-PA (protein: Ub-PA = 1:3) added to UAF1/USP1 sample to a final glycerol concentration of 5%. The mixture was gently stirred and incubated overnight at 4°C. Next, the mixture was loaded onto a Superose 6 Increase 10/300 GL column. The final sample was concentrated to ~3.15 mg/mL in the final buffer: 50-mmol/L Tris-HCl (pH 8.0), 200-mmol/L NaCl, 5% glycerol, and 2-mmol/L Tris (2-carboxy-ethyl)-phosphin-HCl. All cryo-EM samples were applied onto a glow-discharged R1.2/1.3 copper or gold 300-mesh holey carbon grid (Quantifoil) and were immediately frozen in a liquid ethane–propane mixture using a Vitrobot Mark IV (Thermo Fisher Scientific) with the settings at 4°C, 747 95% humidity, and 3 to 6 seconds of blot time.

Cryo-EM sample preparation

For cryo-EM grid preparation, purified USP1/UAF1/Ub-VS sample (0.4 mg/mL concentration) was incubated with 20 μmol/L KSQ-4279 for 1 hour on ice. Aliquots (3.5 mL) of the incubated sample were applied to freshly glow-discharged (70 seconds, 5 W, Plasma Cleaner Glow Discharge) 300-mesh Quantifoil R 1.2/1.3 holey carbon Film Au grids (Quantifoil Micro Tools GmbH). Excess samples were blotted away using filter paper with a blot force of 4, blot time of 3 to 5 seconds, and wait time of 5 seconds and then vitrified by plunge freezing into liquid ethane cooled by liquid nitrogen using Vitrobot Mark IV (Thermo Fisher Scientific) at 4°C and with 100% humidity.

Cryo-EM data collection

The grids were clipped and loaded onto a 300-kV Titan Krios electron microscope (Thermo Fisher Scientific) with an autoloader. Raw movies were collected at a nominal magnification of 105,000 × (pixel size of 0.819 Å) using a K3 camera (Gatan). Inelastically scattered electrons were excluded using a GIF Quantum energy filter (Gatan) with a slit width of 20 eV. The movies were acquired with a defocus range of −1.1 to −1.8 μm, a dose rate of 14.81 e-/(pix·-seconds), an exposure time of 2.5 seconds, and a total dose of 54.8 e-/Å^2 and fragmented into 50 frames. A final dataset of 8,865 movies was semi-automatically collected using EPU software (Thermo Fisher Scientific).

Cryo-EM data processing, model building, and refinement

CryoSPARC V3.2 software package was used for data processing. Patch motion correction was used to correct beam-induced motion correction, and patch CTF estimation was used to calculate CTF parameters, such as defocus and CTF fit resolution. Junk micrographs were discarded by screening parameters, such as CTF fit resolution, ice thickness, and motion distance. In total, 2,791,501 particles were auto-picked and subjected to 2D classification. A total of 691,226 particles with appropriate 2D averages were further subjected to nonuniform refinement. CTF refinement, local refinement, and postprocessing using DeepEMhancer were performed to generate a final map with a resolution of 2.9 Å determined by the gold standard Fourier shell correlation using the 0.143 criterion. The crystal structure of the PDB 7AY2 was used as the initial atomic model. Coot and CCP-EM were used for model building, refinement, and validation.

The PDB and EMD codes for the KSQ-4279 bound structure is [PDB ID: 9DI1, EMD-46895] and for the unbound structure is [PDB ID:9DI2, EMD-46896].

Immunoblot

Cell lysates were prepared in RIPA buffer (Sigma-Aldrich) supplemented with Pierce protease and phosphatase inhibitors (Thermo Fisher Scientific). The samples were incubated for 30 minutes on ice, and the lysates were cleared by centrifugation. Protein concentrations were measured using a Pierce Rapid Gold BCA assay (Thermo Fisher Scientific). Protein samples were diluted in 4× Laemmli sample buffer (Bio-Rad) and denatured at 95°C for 5 minutes. Denatured samples were run on Tris-HCl or Tris-acetate gels (Bio-Rad, Thermo Fisher Scientific) and transferred to nitrocellulose or polyvinylidene difluoride membranes (Thermo Fisher Scientific) using an Invitrogen iBlot system. Membranes were blocked for 1 hour at room temperature in LI-COR Intercept buffer and incubated overnight at 4°C with primary antibodies diluted in intercept buffer containing 0.1% Tween-20. The antibodies used are listed in Supplementary Table S2. The following day, membranes were washed with TBST and incubated for 1 hour at room temperature with secondary antibodies diluted in intercept buffer containing 0.1% Tween-20. Membranes were washed with TBST, and the blots were imaged on an LI-COR-Odyssey CLx.

Clonogenic assays

Cells were seeded in six-well dishes in media conditions as listed in Supplementary Table S1 and incubated overnight. The following day, KSQ-4279 and/or olaparib (SelleckChem) were added at specified concentrations. After 7 days of drug treatment, the media was removed, and fresh media containing the drug was added. On day 14, media was removed, and cells were fixed with 4% paraformaldehyde for 15 minutes. Cells were washed with water and stained with 0.1% crystal violet in a 10% (v/v) ethanol in dH_2O solution for 20 minutes. Plates were washed with water, dried overnight at room temperature, and imaged on an LI-COR Odyssey CLx. Crystal violet was extracted using 10% acetic acid, and absorbance was read using a BioTek Cytation 5 plate reader.

Cleaved caspase-3 staining

MDA-MB-436 cells were seeded in DMEM (Gibco), supplemented with 10% FBS, and incubated overnight. The following day, 0.1% DMSO or 300 nmol/L KSQ-4279 was added to the culture. At the indicated time points, the cells were collected, washed, and resuspended in 100 μL of PBS. A measure of 10 μL of diluted Fixable Viability Dye eFluor 780 (1:200 in PBS; eBioscience) was added to each sample, and the cells were incubated on ice for 20 minutes. Cells were washed with PBS, resuspended in 100 μL of fixation buffer (BioLegend), and incubated for 15 minutes at room temperature. Cells were washed with PBS, resuspended in 100 μL of cold methanol, and stored at −80°C. Upon collection of all samples, the

cells were washed with cell staining buffer (BioLegend), resuspended in 100 μL cell staining buffer containing anti–cleaved caspase-3 antibody (1:5, BD Biosciences, #559341), and incubated on ice for 20 minutes. The cells were washed and resuspended in 100 μL of cell staining buffer. Samples were acquired using an LSR Fortessa X-20 (BD Biosciences) and data were analyzed using FlowJo (v.10.8, BD Biosciences).

DNA fiber assays

Cells were incubated with 50 μmol/L 5-iodo-2′-deoxyuridine (IdU) and 150 μmol/L 5-chloro-2′-deoxyuridine (CldU) sequentially in the presence of the drug, as indicated. Cells were collected and resuspended in PBS at a concentration of 10^5 cells/mL. Cell suspension (2.5 μL) was spotted on a positively charged microscope slide (Globe Scientific, #1358 W) and lysed with 7.5 mL of spreading buffer (0.5% SDS, 200 mmol/L Tris-HCl (pH 7.4), and 50 mmol/L ethylenediaminetetraacetic acid) for 8 minutes at room temperature. Individual DNA fibers were released and spread by tilting the slide at an angle of 45°. After air drying, the fibers were fixed in methanol:acetic acid (3:1) at room temperature for 3 minutes. After air drying, fibers were rehydrated in PBS, denatured with 2.5 mol/L HCl for 30 minutes, washed with PBS, and blocked with blocking buffer (3% BSA and 0.1% Triton in PBS) for 1 hour. Next, the slides were incubated for 2.5 hours with primary antibodies (IdU: 1:100, mouse monoclonal anti-BrdU, Becton Dickinson 347580; CldU: 1:100, rat monoclonal anti-BrdU, Abcam 6326) diluted in blocking buffer, washed several times in PBS, and incubated with secondary antibodies (IdU: 1:200, goat antimouse, Alexa 488; CldU: 1:200, goat antirat, Alexa 594) in blocking buffer for 1 hour. After washing and air drying, the slides were mounted with Prolong (Invitrogen, P36930), and DNA fibers were imaged under a 63× oil immersion lens on a DeltaVision Elite Widefield Deconvolution microscope.

S1 nuclease fiber assay

Cells were incubated with 300nmol/L KSQ-4279 or an equivalent concentration of DMSO for 6 hours, followed by 50-μmol/L IdU and 150-μmol/L CldU sequentially in the presence of the drug or DMSO. Cells were then permeabilized with CSK (cytoskeletal) buffer (100 mmol/L NaCl, 10 mmol/L MOPS (3-(N-morpholino) propane sulfonic acid), 3 mmol/L $MgCl_2$ (pH 7.2), 300 mmol/L sucrose, and 0.5% Triton X-100) at room temperature for 8 minutes and treated with S1 nuclease (20 U/mL) in S1 buffer (30 mmol/L sodium acetate (pH 4.6), 10-mmol/L zinc acetate, 5% glycerol, and 50 mmol/L NaCl) for 30 minutes at 37°C. The cells were collected by scraping, pelleted, and resuspended in 100 to 500 μL of PBS. The cell suspension was spotted on a positively charged slide, lysed, and processed as described in the "DNA fiber assay" section.

pRPA (Ser33) immunofluorescence assay

Cells were seeded on coverslips in a six-well plate in the respective media conditions and incubated overnight. The following day, compounds were added, and cells were incubated as indicated. Following treatment, cells were washed with PBS and preextracted with 0.5% Triton X-100 in PBS for 5 minutes on ice. Cells were then fixed with 4% paraformaldehyde for 15 minutes at room temperature. The fixed cells were incubated with primary antibodies against pRPA S33 (1:250 NB100-544) at 37°C for 1 hour. The cells were washed and incubated with secondary Abs (1:250 Alexa Fluor 488 goat anti–rabbit IgG) for 1 hour at room temperature. After washing, the coverslips were mounted onto glass slides using a Vectashield mounting medium containing 4′,6-diamidino-2-phenylindole (DAPI; Vector Laboratories). Images were taken under a 60× oil immersion lens on a DeltaVision Elite Widefield Deconvolution microscope for analysis.

PARylation assay

Cells were seeded on coverslips in a six-well plate using the respective media conditions and incubated overnight. The following day, 10-μmol/L PARGi (Sigma-Aldrich SML1781) was added to either KSQ-4279 or hydroxyurea (Sigma-Aldrich H8627), and cells were incubated for an additional 30 minutes. After treatment, cells were washed with PBS, fixed with 4% formaldehyde in PBS for 10 minutes at room temperature, and subsequently permeabilized by a 5-minute incubation in ice-cold methanol/acetone solution (1:1). After blocking the cells with 10% fetal calf serum for 30 minutes, coverslips were incubated with an anti-PAR polyclonal antibody (1:250 Trevigen 4336-BPC-100) at 37°C for 1 hour. After washing with PBS, cells were incubated with Alexa Fluor 488 goat antirabbit antibody (1:200) for 1 hour at room temperature. After washing, the coverslips were mounted onto glass slides using Vectashield mounting medium with DAPI (Vector Laboratories). Images were taken under a 60× oil immersion lens on a DeltaVision Elite Widefield Deconvolution microscope for analysis.

Animal studies

Mice were housed in ventilated cage systems in pathogen-free animal facilities. Animal rooms were maintained under a 14/10 or 12-hour light-dark cycle, with temperature and humidity ranges maintained within the recommended guidelines. Mice were allowed to acclimatize for at least 72 hours prior to study enrollment, with access to food and water *ad libitum*. All procedures involving the care and use of animals were performed with approval from and under the guidance of the Institutional Animal Care and Use Committee or the relevant animal ethics committee.

Subcutaneous tumor models

Four-to-seven-week-old female BALB/c nude or Athymic Nude-Foxn1^{nu} mice were purchased from Beijing Anikeeper Biotech Co., Ltd., or Envigo, respectively. Tumor fragments from stock mice were harvested and approximately 2-to-5-mm fragments were injected subcutaneously into the left or right flank of mice for tumor development. Once tumors reached at least 100-mm^3 mice were randomized by tumor volume and body weight into cohorts for treatment initiation. Tumors were measured at least twice weekly using a manual caliper, and tumor volume (mm^3) was calculated using the following formula: $V = 0.5 \times (a \times b^2)$ in which a and b are the long and short diameters of the tumor, respectively. Body weight was measured at least twice per week and the mice were monitored daily for clinical signs of toxicity. Changes in body weight compared with pretreatment body weight (day 0) were calculated using the following formula: (BW Day X/BW Day 0 × 100)−100.

Orthotopic ovarian tumor models

Human tumor ascites or pleural effusions were collected from patients, and luciferase-tagged patient-derived xenograft (PDX) models were generated by the Dana-Farber Cancer Institute, as previously described (20). Seven-week-old female NOD/SCID *IL2Rγ^{null}* mice were purchased from The Jackson Laboratory, and approximately 5×10^6 luciferized PDX tumor cells prepared in PBS were injected intraperitoneally into the abdomen for tumor

development. Mice were imaged, and once bioluminescence reached between 3 and 5 × 10^8 (photons/seconds/cm^2/sr) were randomized into cohorts for treatment initiation. Serial imaging was performed weekly using bioluminescence to assess disease burden, and body weights were recorded twice weekly.

IHC evaluation of mouse tumors

Freshly collected tumor tissues were placed in 10% neutral buffered formalin and fixed for 24 hours at room temperature. The tumor tissues were then trimmed to 3 to 5 mm. After rinsing with running water, the tissues were transferred to a vacuum tissue processor (HistoCore PEARL, Leica) for dehydration and then embedded into formalin-fixed, paraffin-embedded tissue blocks using a tissue embedding center (EG1150, Leica). For slide preparation, formalin-fixed, paraffin-embedded blocks were sectioned at a thickness of 4 μm using a manual rotary microtome (HistoCore MULTICUT, Leica). IHC staining was performed using the following antibodies: Ubiquityl-PCNA Lys164, Clone D5C7P (Cell Signaling, 13439). All stained sections were scanned with a panoramic digital slide scanner (3DHISTECH, Pannoramic SCAN) with high-resolution pictures generated for whole sections. All images were analyzed using the HALO platform, and the intensity of IHC staining was scored at four levels: 0 (negative), 1 (weak staining), 2 (medium staining), and 3 (strong staining). The percentage of tumor cells at different intensity levels was evaluated and an overall H-score was generated using the following formula: H-score = (% cells at 0) × 0 + (% cells at 1) × 1 + (% cells at 2) × 2 + (% cells at 3) × 3.

LC/MS-MS determination of KSQ-4279

The plasma and tumor concentrations of KSQ-4279 were determined using qualified LC/MS-MS method. Briefly, plasma samples were protein precipitated with acetonitrile containing dexamethasone, the internal standard, vortex-mixed, and centrifuged. Tumors were weighed and homogenized (at 4°C in a wet ice-containing water bath) with water at a tissue weight (g) to water volume (mL) ratio of 1:10 before analysis. An aliquot of the supernatant was diluted and injected into a Shimadzu liquid chromatography system. Analytes were separated by a Phenomene × Kinete × 50 × 2.1 mm, 5μm C18 100 Å column, with a gradient mobile phase consisting of a mixture of 5% acetonitrile in water with 0.1% formic acid and 95% acetonitrile in water with 0.1% formic acid. Analytes were detected using an API 5500 (Applied Biosystems) mass spectrometer operated in positive turbo ion spray mode with selective reaction monitoring of KSQ-4279 and the internal standard.

Statistical analysis

Statistical analyses in the DNA fiber assay, S1 nuclease assay, and immunofluorescence assays were performed using a two-tailed Mann–Whitney test. Statistical analyses were performed using Microsoft Excel and GraphPad Prism software (version 9.0). In all cases, NS indicates no significance, $P > 0.01$; *, $P < 0.05$; **, $P < 0.01$; ***, $P < 0.001$; and ****, $P < 0.0001$.

Data availability

The data generated in this study are available upon reasonable request and should be made directly to datasharingrequest@ksqtx.com.

Results

Specific subsets of cancer cell lines are dependent on the USP1/UAF1 deubiquitinase complex

To identify novel therapeutic targets that exploit key vulnerabilities associated with tumor growth and survival, we performed full genome, CRISPR/Cas9 screens across >500 cancer cell lines to generate a database that provided a comprehensive insight into the genetic dependency profile of each cell line. Mining this dataset for novel targets that are selectively essential and share a putative biomarker, rather than exhibiting broad cytotoxicity, led to the identification of USP1 and its heterodimerization partner UAF1 (**Fig. 1A**; Supplementary Fig. S1; Supplementary Table S3). The USP1/UAF1 complex is a key regulator of the TLS and FA pathways, both of which play key roles in DNA repair processes (21–23). Profiling of USP1/UAF1 dependent cell lines for putative biomarkers revealed there was an enrichment of ovarian and breast cancer lineages. High-grade serous ovarian cancer and triple-negative breast cancer (TNBC) are often characterized by alterations in the HR pathway, including mutations in *BRCA1* and *BRCA2* (24–26), raising the possibility of a synthetic lethal relationship between USP1/UAF1 loss and the presence of *BRCA* mutations or HR pathway alterations. HR-deficient basal-like breast cancer samples have significantly higher expression levels of USP1 than other breast cancer subtypes, and USP1 expression was also enriched in BRCA1-mutant ovarian cancers that were resistant to platinum agents (27). The same studies have also shown that USP1 is required for the stabilization of replication forks in BRCA1-deficient tumors (21). Clinically, approximately 25% of patients with high-grade serous ovarian cancer and 10% to 20% of patients with TNBC have mutations in either *BRCA1* or *BRCA2*, with the frequency of patients with a broader defect in the HR pathway rising to over 50% of ovarian cancer and almost 25% of patients with breast cancer (11, 28, 29). The enrichment of these cancer cell line lineages in the USP1 dependency subset and the reported role of USP1 in BRCA1-deficient cells indicate that defects in HR may create a dependency on pathways that are regulated by USP1 and may thus represent a promising target for therapeutic intervention.

Discovery of KSQ-4279, a potent and selective USP1 inhibitor

The development of potent, selective inhibitors that target DUBs, such as USP1, has proven to be challenging because of the conserved nature of the catalytic pocket across the DUB family, with no DUB inhibitors currently approved for therapeutic use (30). To develop a USP1 inhibitor with the necessary selectivity and drug-like properties for clinical testing, a comprehensive medicinal chemistry campaign was launched, which ultimately led to the identification of KSQ-4279 (**Fig. 1B**).

KSQ-4279 potently inhibits the DUB activity of USP1 with an affinity of 2 nmol/L (**Fig. 1C**) and demonstrates excellent selectivity for USP1 when tested across a panel of 43 DUBs (**Fig. 1D**). Enzyme kinetic studies demonstrate reversible binding (Supplementary Fig. S2) and show a clear decrease in V_{max} (**Fig. 1C**), eliminating a simple competitive inhibition mechanism. Secondary plots of V_{max}, K_m, and V_{max}/K_m all decrease in a hyperbolic manner (Supplementary Fig. S2), with an excellent global fit to a mixed linear inhibition mechanism. The kinetic data indicate that KSQ-4279 binds to an allosteric pocket with a moderately tighter affinity (~3-fold) in the presence of the ubiquitin–rho substrate than USP1 alone.

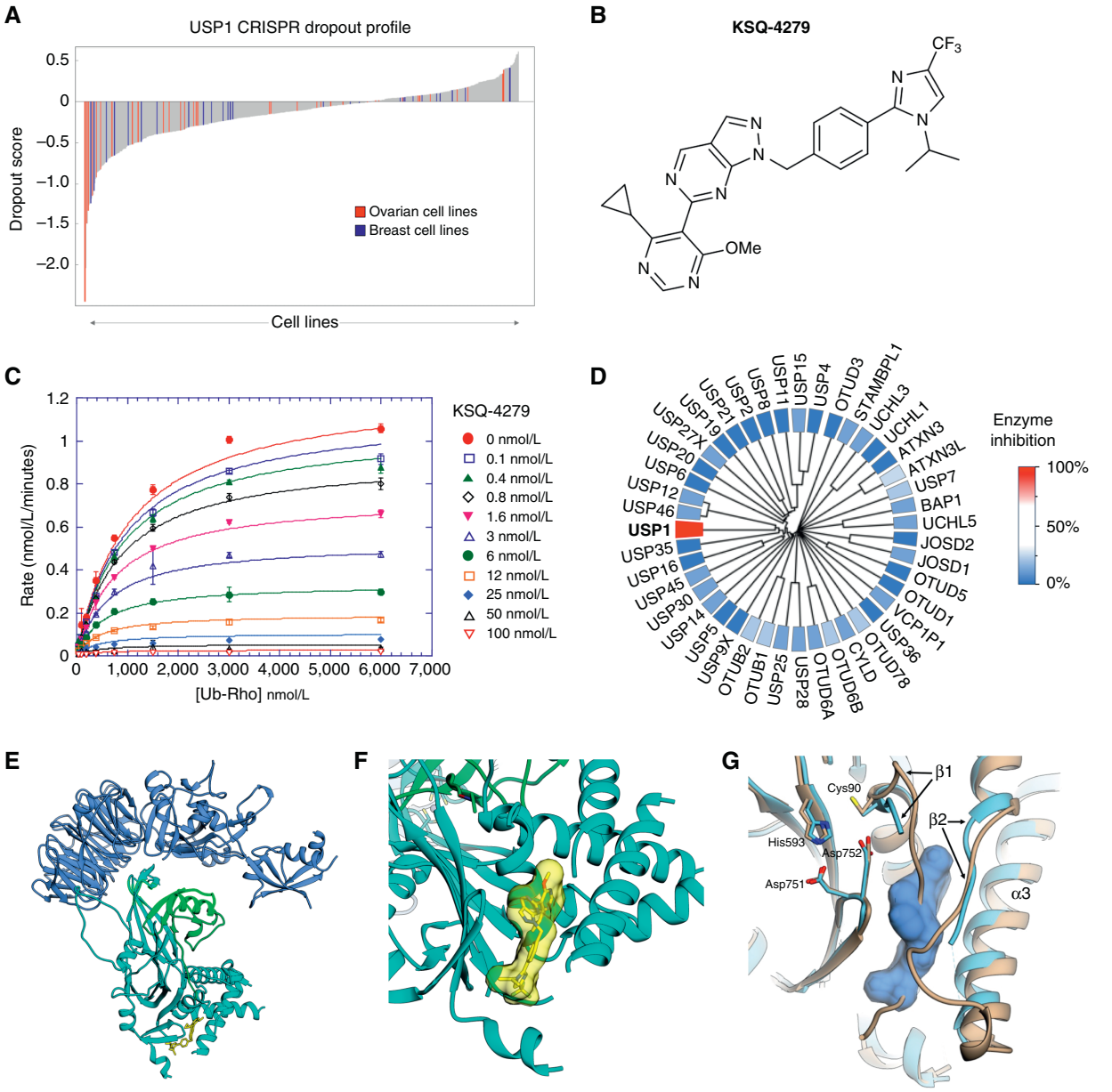

Figure 1.

A, USP1 dependency profile using a CRISPR knockout screen across >500 cell lines. **B,** Chemical structure of KSQ-4279. **C,** KSQ-4279 binding affinity was determined by measuring the initial rate dependence of USP1 with Ub-Rho substrate as a function of fixed increasing concentrations of KSQ-4279. Solid lines are simulated from the mixed linear inhibition model global fit parameters: V_{max} 1.24 (±0.04) nmol/L minutes^{-1} (k_{cat} = 0.82 seconds^{-1}), K_m = 1,038 (±90) nmol/L, K_{ic} = 6.9 (±3) nmol/L, and K_{iu} = 2.3 (±0.3) nmol/L. Points averaged from N = 4 determinations. Error bars, SD. **D,** Selectivity assessment of KSQ-4279 was established by testing a panel of deubiquitinases using a ubiquitin–rhodamine biochemical assay using 1-μmol/L KSQ-4279. **E,** Cryo-EM structure of the KSQ-4279 inhibited USP1–UAF1–ubiquitin complex. USP1, UAF1, and ubiquitin are rendered as cyan, blue, and green ribbons, respectively. KSQ-4279 is depicted as a yellow stick. **F,** KSQ-4279 shown inside a semitransparent molecular surface as it is cradled by the palm and thumb subdomains of USP1. **G,** USP1-apo (brown) is rendered as a ribbon superposed on the USP1/KSQ-4279 ribbon structure (light blue). KSQ-4279 is depicted as a blue molecular surface.

The cryo-EM structure of the USP1–UAF1–ubiquitin complex in both the KSQ-4279-bound (PDB ID: 9DI1) and unbound (PDB ID: 9DI2) states was determined at a resolution of 2.6 Å (**Fig. 1E–G**; Supplementary Figs. S3 and S4). Cryo-EM structures revealed that KSQ-4279 binds to an allosteric pocket in the hydrophobic core of USP1 that, notably, is not present in the unbound USP1 structure, indicating that KSQ-4279 binds through an induced-fit mechanism. This region is not conserved across other DUBs and likely explains why KSQ-4279 is highly selective for USP1, relative to other family members. Comparison of the bound and unbound structures indicates that KSQ-4279 displaces and disorders the β2 strand running from Gln160 to Thr176, with the β1 strand segment from Thr89 to

Glu75 undergoing similar perturbations up to Cys90, which serves as the key catalytic cysteine required for deubiquitination of substrates. This indicates a molecular inhibition mechanism whereby KSQ-4279 binds to the hydrophobic core of USP1, leading to conformational changes that result in the misalignment of Cys90, thus preventing the catalytic removal of ubiquitin from the substrate.

Cellular and *in vivo* activity of KSQ-4279–mediated USP1 inhibition

The TLS and FA pathways are DNA repair processes regulated by USP1 through the deubiquitination of monoubiquitinated PCNA (Ub-PCNA) and monoubiquitinated FANCD2 (Ub-FANCD2), respectively (21–23). In the BRCA1-mutant cell line MDA-MB-436, KSQ-4279 induced the accumulation of both Ub-PCNA and Ub-FANCD2 in a dose-dependent manner (**Fig. 2A**). Across a time course of treatment, KSQ-4279 led to a rapid accumulation of both mono- and poly-Ub-PCNA in the first 24 hours, followed by a reduction of Ub-PCNA, which coincided with reductions in the levels of total PCNA (**Fig. 2B**). Similarly, Ub-FANCD2 levels increased at early time points and showed a gradual decrease over the following days. In addition, KSQ-4279 treatment led to increased levels of pCHK1 and pH2AX, markers of replication stress and DNA damage induction (31, 32), and triggered apoptosis, as indicated by an increase in cleaved caspase-3 (**Fig. 2C**; ref. 33). To determine how this cascade of signaling events affects the growth and survival of the cells, KSQ-4279 was tested in clonogenic assays across a dose range. Clonogenic cell growth was inhibited by KSQ-4279 at doses consistent with those that induced the accumulation of monoubiquitinated substrates and DNA damage markers (**Fig. 2D**). A panel of cell lines that the CRISPR screen identified as differentially dependent on USP1 was used to determine whether the sensitivity to KSQ-4279 matched the genetic dependency on USP1. Clonogenic assays confirmed that sensitivity to KSQ-4279 correlated closely with USP1 dependency after CRISPR knockout (**Fig. 2E**).

Next, we assessed whether KSQ-4279 was active *in vivo* using PDX models. To ensure consistent bioavailability and exposure following oral dosing, KSQ-4279 was administered as a KSQ-4279: gentisic acid cocrystal (1:1). In the BRCA1-mutant ovarian PDX OV0589, oral administration of KSQ-4279 to mice led to a dose-dependent increase in plasma and tumor exposures (**Fig. 3A**). To relate the exposure of KSQ-4279 to the inhibition of USP1 in the tumor, Ub-PCNA levels were monitored using IHC, and the staining frequency and intensity were quantified to generate an *H*-score (**Fig. 3B**; Supplementary Fig. S5). Following a single dose of KSQ-4279, Ub-PCNA levels increased as early as 4 hours across all doses but started to decrease at 24 hours postdose at the lower (10 and 30 mg/kg) dosing levels. In contrast, a sustained increase in Ub-PCNA was observed across the 24-hour timeframe at 100 and 300 mg/kg KSQ-4279. To determine how this PK/PD relationship translated into antitumor activity in the OV0589 ovarian PDX model, KSQ-4279 was dosed orally once a day for >10 weeks across the same range of doses. From a safety perspective, KSQ-4279 was well tolerated with no overt signs of toxicity and minimal to no body weight loss observed (Supplementary Fig. S6). At lower doses of KSQ-4279 (10 and 30 mg/kg), only partial inhibition of tumor growth was observed; however, at higher dose levels of 100 and 300 mg/kg, KSQ-4279 exhibited clear antitumor activity with tumor regression noted (**Fig. 3C**).

Sensitivity to KSQ-4279 is mediated by PCNA ubiquitination

To understand the mechanistic basis for the antitumor activity of KSQ-4279, we first investigated whether the sensitivity of HR-deficient cells was mediated by the accumulation of Ub-PCNA and/or Ub-FANCD2 (**Fig. 4A**). Expression constructs containing point mutations that prevent monoubiquitination of $PCNA^{(K164R)}$ or $FANCD2^{(K561R)}$ were introduced into the HR-deficient CAOV3 cells. Although cells expressing $FANCD2^{(K561R)}$ remained sensitive to KSQ-4279, the expression of $PCNA^{(K164R)}$ rendered these cells insensitive to KSQ-4279, suggesting that Ub-PCNA levels are linked to the sensitivity to KSQ-4279 (**Fig. 4B**). This hypothesis was further tested by knocking out the E3 ligase *RAD18*, which is responsible for monoubiquitination of PCNA (34, 35). Inactivation of *RAD18* reduced the levels of Ub-PCNA and rendered CAOV3 cells insensitive to KSQ-4279 (**Fig. 4C**). Together, these findings indicate that Ub-PCNA, but not FANCD2, is involved in mediating the antiproliferative effects of KSQ-4279 in HR-deficient cells.

We previously observed that sustained monoubiquitination of PCNA, as a result of USP1 inhibition, was followed by a reduction in the total PCNA levels (**Fig. 2B**). Consistent with a previous report (36), we also observed that USP1 sensitivity generally correlated with a reduction in total PCNA levels (Supplementary Fig. S7). To understand whether total PCNA loss may be driving the replication stress induced by KSQ-4279 or merely represents a consequence of it, we monitored the kinetics of PCNA degradation relative to the phosphorylation of CHK1 (S345) across a panel of KSQ-4279 sensitive cell lines. In each cell line, pCHK1 (S345) levels increased 3 hours after treatment with KSQ-4279, whereas PCNA degradation was only observed at later time points ranging from 6 to 16 hours (**Fig. 4D**). These findings suggest that cells sensitive to KSQ-4279 experience replication stress before PCNA degradation occurs.

KSQ-4279 treatment leads to ssDNA gap induction and loss of replication fork integrity

To investigate which mechanisms might be inducing replication stress, we evaluated the impact of KSQ-4279 on replication fork dynamics using the DNA fiber assay. Replication fork stability was monitored by sequentially labeling the cells with the nucleotide analogs IdU and CldU, followed by treatment with KSQ-4279 for 6 hours. Fork degradation was observed in cells sensitive to KSQ-4279, with no evidence of fork degradation in cells insensitive to KSQ-4279 (**Fig. 5A**). Similar to the role of RAD18 in Ub-PCNA and the antiproliferative effects of KSQ-4279, inactivation of *RAD18* rescued the fork degradation induced by KSQ-4279. We next investigated whether KSQ-4279 disrupted the normal process of replication and thereby contributed to fork instability by assessing DNA tract lengths. After 6 hours of KSQ-4279 treatment, cell lines known to be sensitive to KSQ-4279 displayed longer DNA tract lengths than DMSO-treated cells, an effect that was not observed when cells were insensitive to KSQ-4279 treatment. (**Fig. 5B**). However, this initial fork lengthening was not sustained, as cells treated with KSQ-4279 for 24 hours displayed shorter DNA tracts than those treated with DMSO.

Treatment of cells with the PARP inhibitor olaparib has been reported to accelerate replication fork speed, resulting in longer DNA fibers and consequently leading to ssDNA gap accumulation (37, 38). We hypothesized that treatment with KSQ-4279 might similarly dysregulate replication fork dynamics and result in ssDNA gap accumulation. To investigate this, cells that showed longer DNA tracts upon treatment with KSQ-4279 were subjected to S1 nuclease cleavage (39). Treatment with S1 nuclease significantly decreased the DNA tract length, suggesting the presence of ssDNA gaps along the newly

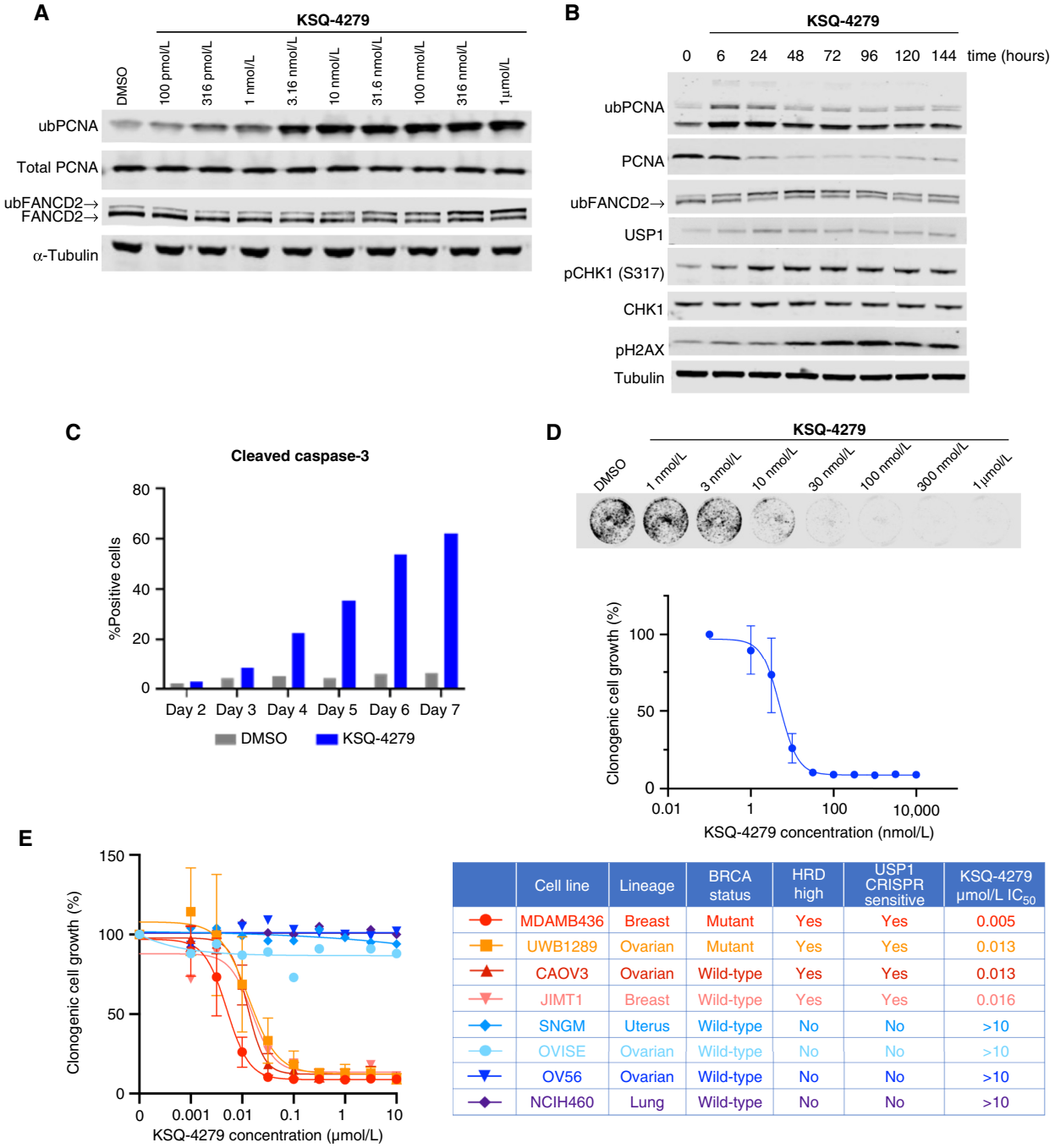

	Cell line	Lineage	BRCA status	HRD high	USP1 CRISPR sensitive	KSQ-4279 µmol/L IC_{50}
●	MDAMB436	Breast	Mutant	Yes	Yes	0.005
■	UWB1289	Ovarian	Mutant	Yes	Yes	0.013
▲	CAOV3	Ovarian	Wild-type	Yes	Yes	0.013
▼	JIMT1	Breast	Wild-type	Yes	Yes	0.016
◆	SNGM	Uterus	Wild-type	No	No	>10
●	OVISE	Ovarian	Wild-type	No	No	>10
▼	OV56	Ovarian	Wild-type	No	No	>10
◆	NCIH460	Lung	Wild-type	No	No	>10

Figure 2.

A, Immunoblot analysis of MDA-MB-436 cells treated with a dose titration of KSQ-4279 for 6 hours. **B,** MDA-MB-436 cells treated with 300-nmol/L KSQ-4279 across a time course to assess pharmacodynamic response and DNA damage induction. **C,** Cleaved caspase-3 expression in MDA-MB-436 cells treated with either 300-nmol/L KSQ-4279 or DMSO over a 7-day time course. **D,** KSQ-4279 induced growth inhibition of MDA-MB-436 cells as assessed via clonogenic assays. Data are representative of three independent experiments, with one representative example shown. **E,** KSQ-4279 induced growth effects across a panel of cell lines as assessed via clonogenic assays.

synthesized DNA (**Fig. 5C**). This finding was corroborated by an increase in the formation of pRPA (Ser33) foci, a marker for ssDNA, upon KSQ-4279 treatment in sensitive cells relative to insensitive cells (**Fig. 5D**).

Failure to repair ssDNA lesions can lead to DSBs and activate cell death pathways (40, 41). PARP1-induced PARylation functions as a DNA damage sensor and is required to initiate ssDNA repair (42–44); thus, PAR levels were examined to indicate the presence of ssDNA

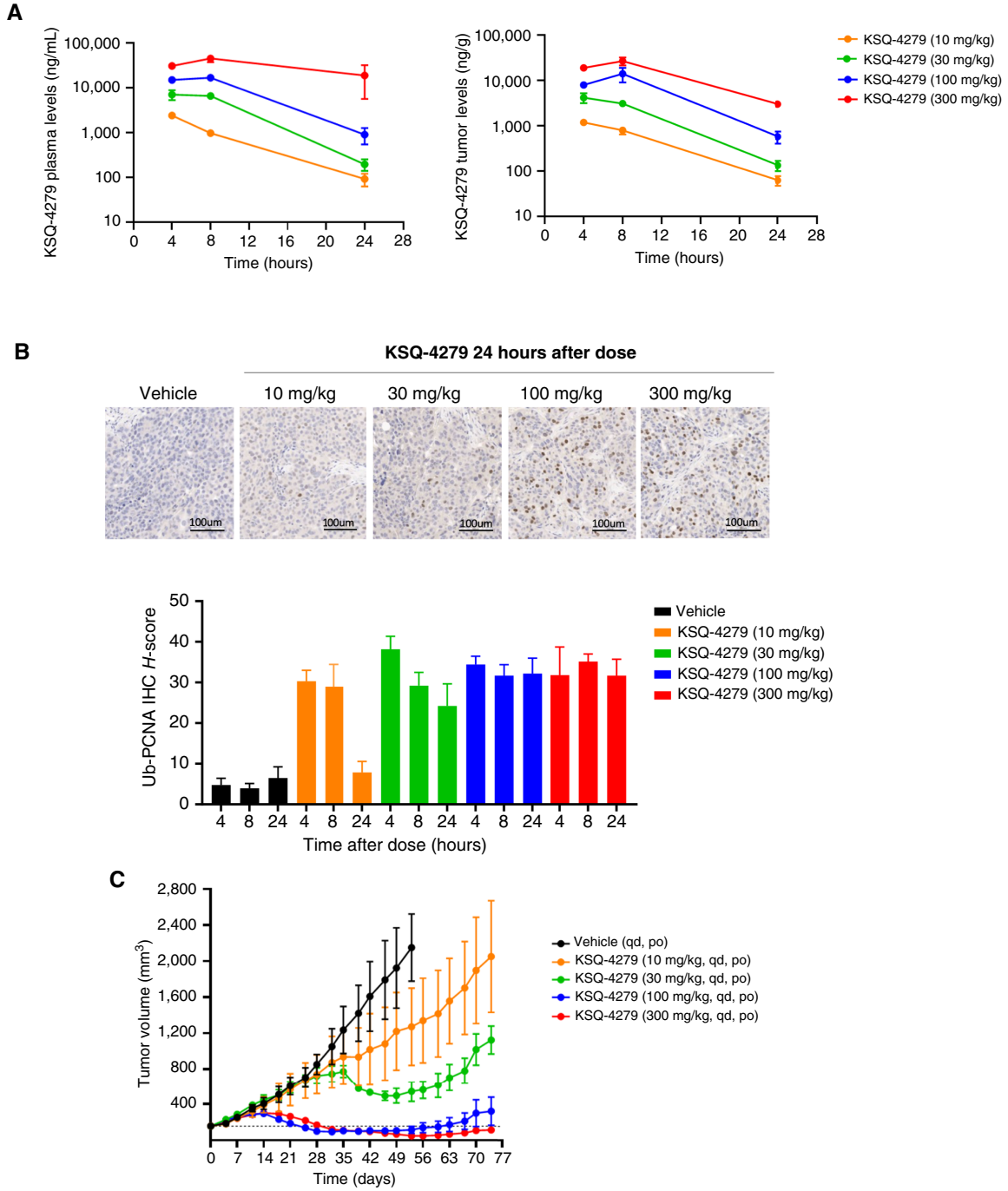

Figure 3.

A, KSQ-4279 plasma and tumor exposure was determined at 4, 8, and 24 hours following a single oral dose administered at 10, 30, 100, or 300 mg/kg. **B,** Tumors were collected at 4, 8, or 24 hours after single dose of control or KSQ-4279, formalin-fixed, paraffin-embedded, sectioned, and stained for Ub-PCNA, and representative images are shown. Scale bar, 100 μm. IHC *H*-score was established based on percentage of positive cells and intensity of Ub-PCNA staining. **C,** Tumor growth curve for OV0589 human ovarian PDX model treated with per oral once daily 10 mL/kg control, 10-, 30-, 100-, or 300-mg/kg KSQ-4279. Mice (n = 3/group) were randomized, and treatment administered once the mean tumor volume reached approximately 200 mm^3, denoted as day 0. The dotted black line represents the mean tumor volume in the combination-treated group on day 0, prior to treatment initiation. qd, once daily; po, orally.

gaps. KSQ-4279-treated cells showed an enhanced degree of PAR build-up, corroborating the observations from the S1 nuclease and pRPA foci formation assays (**Fig. 5E**). Collectively, our data suggest that in USP1-dependent cell lines, treatment with KSQ-4279 results in replication fork dysregulation, ssDNA gap accumulation, and loss of replication fork integrity, which collectively leads to cell death.

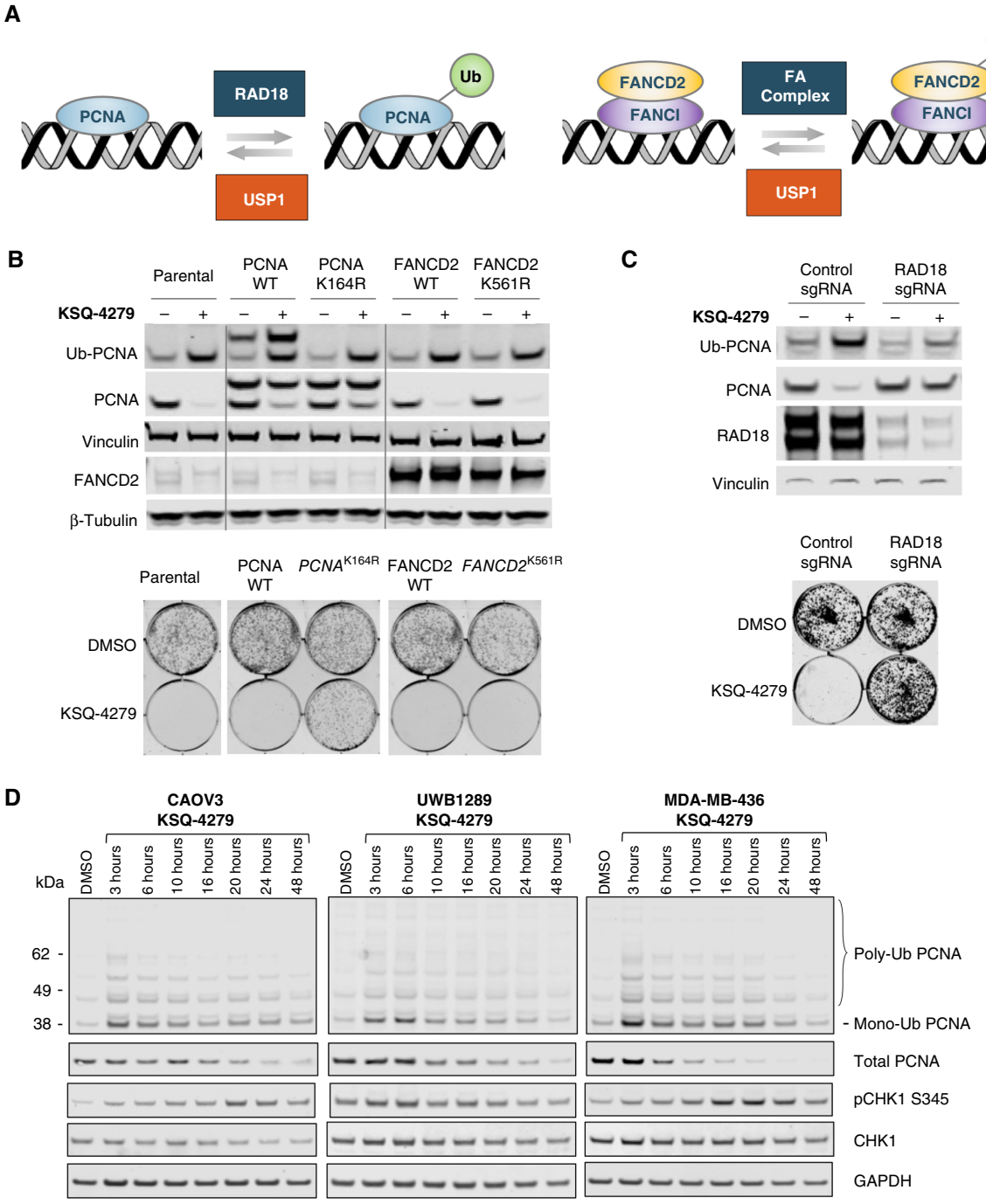

Figure 4.

A, Schematic overview of the ubiquitination and deubiquitination of the USP1 substrates, PCNA, and FANCD2. **B,** Top, immunoblot analysis of CAOV3 cells engineered to overexpress PCNA and FANCD2 constructs after treatment with 300 nmol/L KSQ-4279. Note that the PCNA constructs contained a Flag-tag, which runs as the upper band in the PCNA blots. Bottom, 14-day clonogenic assays to determine the impact of the point mutations on the sensitivity to KSQ-4279. **C,** Top, immunoblot analysis of CAOV3 cells containing CRISPR knockout of RAD18 after treatment with KSQ-4279. Bottom, 14-day clonogenic assay results showing differential responses to 300 nmol/L KSQ-4279. **D,** Immunoblot analysis of cells treated with 300 nmol/L KSQ-4279 across a range of time points showing the impact of USP1 inhibition on PCNA and CHK1 levels.

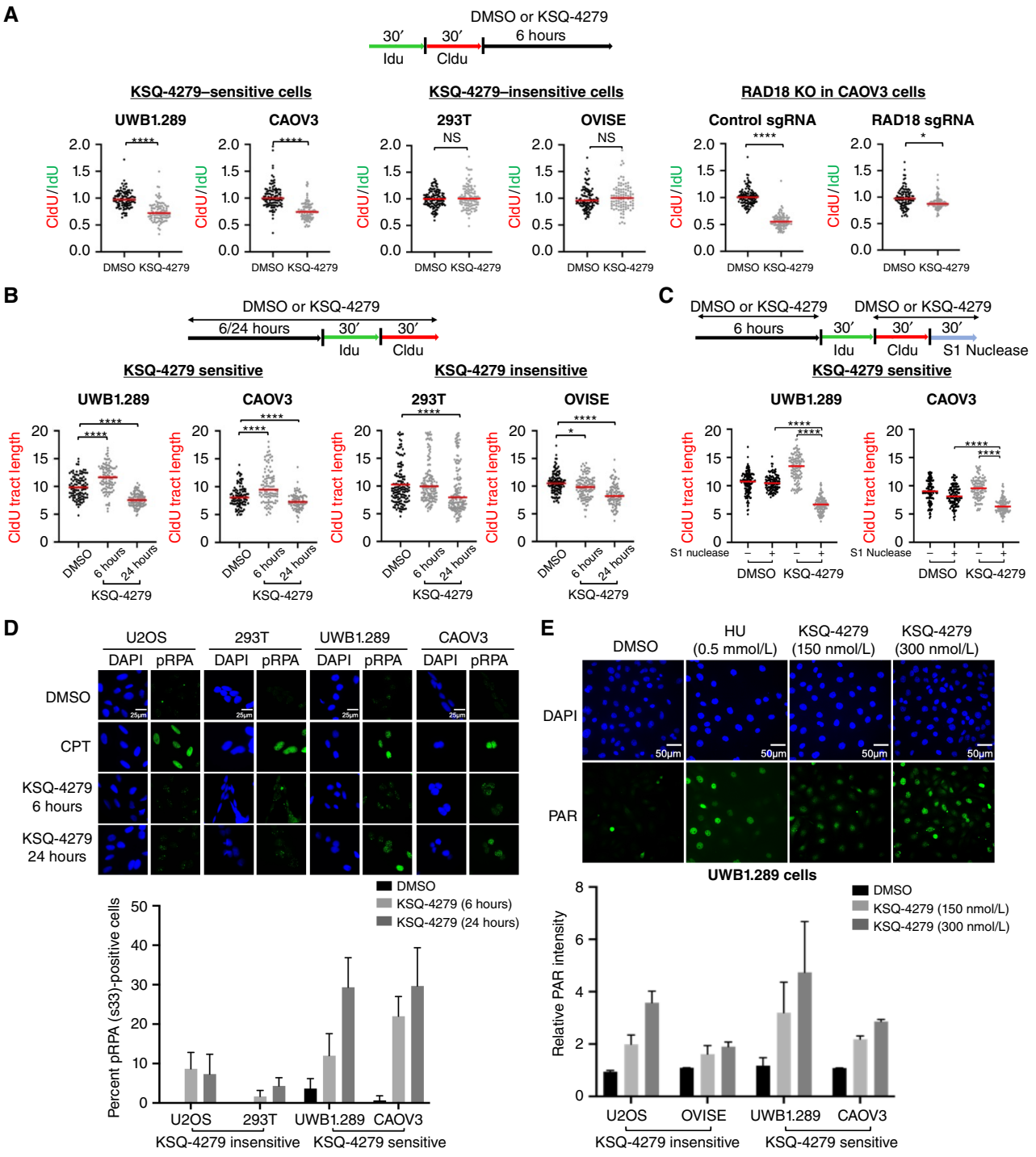

Figure 5.

A–C, DNA fiber assays were performed to study the impact of KSQ-4279 on replication fork stability, replication fork progression, and the presence of ssDNA gaps in nascent DNA fibers. For each experiment, the drug treatment and CldU/IdU incorporation schedules are illustrated. Each dot represents one fiber and between 100 and 200 fibers are quantified from two independent experiments. Bars, means ± SD. Statistical analysis was performed according to the two-tailed Mann–Whitney test. **D,** Representative images of cells stained for DAPI and phospho-RPA(Ser33) upon treatment with DMSO, 10-μmol/L camptothecin (CPT) for 24 hours, and 300 nmol/L KSQ-4279 for 6 and 24 hours. Images were taken at 60× oil immersion and foci quantified. Data were collected by running replicates in two independent experiments. **E,** Representative images of UWB1.289 cells stained for DAPI and PAR upon treatment with DMSO, 0.5 mmol/L hydroxyurea (HU), and different doses of KSQ-4279 in the presence of 10 μmol/L PARGi for 30 minutes. Images were taken at 60× oil immersion and PAR intensity quantified. Data were collected by running replicates in two independent experiments. *, $P < 0.05$; ****, $P < 0.0001$.

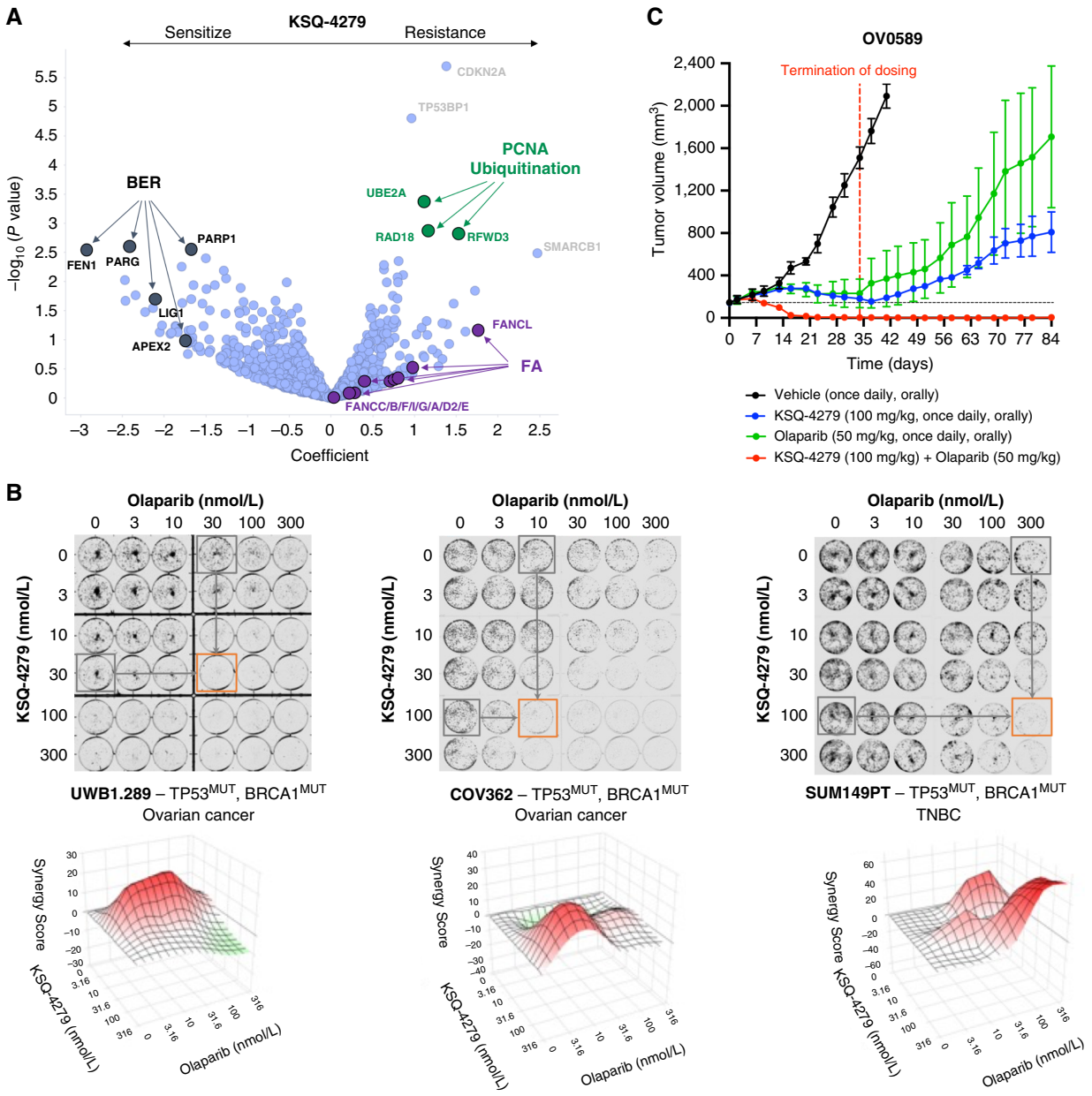

Figure 6.

A, A DDR-enriched CRISPR library was used to run a CRISPR/Cas9 functional genomics screen in UWB1.289 cells in the presence or absence of 300 nmol/L KSQ-4279. Cells were harvested, genomic DNA isolated, and deep sequencing performed to identify which guides were enriched or depleted from the cells. **B,** Clonogenic assay results in a panel of BRCA-mutant cell lines after 14-day combination treatments of KSQ-4279 and olaparib. **C,** Tumor growth curves for the PDX model, OV0589, treated once daily via oral gavage, with vehicle control, 100 mg/kg KSQ-4279, 50-mg/kg olaparib or the combination of 100 mg/kg KSQ-4279, and 50 mg/kg olaparib. Mice ($n = 3$/group) were randomized and treatment administered once the mean tumor volume reached approximately 200 mm^3, denoted as day 0. The horizontal dotted black line represents the mean tumor volume in the combination-treated group on day 0, prior to treatment initiation. Compounds were administered once daily for 34 days, at which point, dosing was terminated (dotted red line) and tumor size monitored.

USP1 inhibition in BRCA1-mutant cells creates a dependency on PARP1 and the BER pathway

Given the ssDNA gap accumulation and replication stress induced by KSQ-4279, we next determined which specific DNA repair pathways intersect with these processes and influence the sensitivity of cells to KSQ-4279. To this end, we performed a CRISPR/Cas9 screen in the presence and absence of KSQ-4279 in the BRCA1-mutant ovarian cancer cell line, UWB1.289 (**Fig. 6A**). The data from this screen further corroborated our earlier findings that inactivation of pathways involved in the ubiquitination of PCNA (RAD18, UBE2A, and RFWD3; refs. 45–47) reduced the sensitivity of the cells to KSQ-4279, with genes involved in the FA pathway having a more

modest impact. In contrast, analysis of the dataset for gene knockouts that sensitize cells to KSQ-4279 revealed several genes involved in the BER pathway, including PARP1, the target of multiple approved therapies (48). Consistent with the genetic sensitizer screen results, we found that the PARP inhibitor olaparib showed strong combination activity with KSQ-4279 in both BRCA1-mutant, HR-deficient ovarian, and TNBC cell lines (**Fig. 6B**). Importantly, the combination of olaparib and KSQ-4279 seemed to be selective for BRCA-mutant/HR-deficient cells, as several *BRCA1*^{WT}/HR-proficient cell lines were unaffected under the same assay conditions (Supplementary Fig. S8). This combination effect was not limited to olaparib but was also observed with both PARP-trapping agents, such as niraparib and talazoparib, and the more recently developed PARP1-selective inhibitor, AZD5305 (49), in addition to the non–PARP-trapping agent, veliparib (Supplementary Fig. S9). These findings indicated that the combination of KSQ-4279 and PARP inhibitors is enhanced in tumors with BRCA/HR defects.

To evaluate whether the *in vitro* combination benefit of KSQ-4279 and PARP inhibitors translated to an *in vivo* setting, tumor efficacy studies were performed across multiple ovarian and TNBC PDX models. In the ovarian BRCA1-mutant PDX model OV0589, dosing with KSQ-4279 (100 mg/kg) and olaparib (50 mg/kg) as single agents was efficacious, but tumors quickly relapsed when dosing was stopped (**Fig. 6C**). However, when KSQ-4279 (100 mg/kg) and olaparib (50 mg/kg) were administered in combination, all mice demonstrated pronounced and sustained tumor regression. Strikingly, although all animals treated with single agents relapsed following the termination of dosing on day 34, no tumor outgrowth was observed in any of the mice that received a combination of KSQ-4279 and olaparib.

KSQ-4279/olaparib combinations can overcome PARPi resistance

Although PARP inhibitors provide significant benefits to patients with BRCA-mutant/HR-deficient tumors, the development of both *de novo* and acquired resistance presents a major clinical challenge (50). To test the activity of KSQ-4279/olaparib combinations in the PARP refractory setting, we identified Ovarian and TNBC PDX models that closely resembled the clinical setting in which, despite the presence of a pathogenic BRCA1 mutation, the tumors were HR-proficient and resistant to PARPi (51). One such model is the TNBC PDX model, HBCx-8, in which neither olaparib (100 mg/kg) nor KSQ-4279 (100 mg/kg) were active when dosed as single agents; however, the combination of KSQ-4279 (100 mg/kg) and olaparib (100 mg/kg) was striking in its ability to control tumor growth (**Fig. 7A**). Importantly, the combination of KSQ-4279 and olaparib was well tolerated for over 2 months of dosing, with no overt signs of toxicity and minimal to no body weight loss observed (Supplementary Fig. S6). Similarly, the combination of KSQ-4279 (100 mg/kg) and olaparib (50 mg/kg) was active in the TNBC PDX model, HBCx-11, and in the ovarian PDX model, CTG-0703, KSQ-4279 (100 mg/kg), and olaparib (100 mg/kg) were active in combination despite each agent alone having limited to no effects on tumor growth (**Fig. 7A**).

Next-generation PARP1-selective inhibitors, such as AZD5305, are currently being developed with the goal of increasing their efficacy and tolerability compared with first-generation PARP inhibitors. Using the PARP-resistant HBCx-8 model that we previously tested with olaparib, we tested 10-mg/kg AZD5305 as a single agent and in combination with 100-mg/kg KSQ-4279. AZD5305 (10 mg/kg) as a single agent resulted in only mild antitumor activity; however, the combination of AZD5305 (10 mg/kg) and KSQ-4279 (100 mg/kg) induced durable tumor regressions (**Fig. 7B**). Of note, the combination of AZD5305 and KSQ-4279 showed stronger regressions than those observed with olaparib/KSQ-4279 (**Fig. 7A**), indicating that KSQ-4279 combinations with next-generation PARP1-selective inhibitors may further increase the therapeutic benefit. Next, we tested whether mice that progressed on AZD5305 as a single agent remained sensitive to the combination of KSQ-4279 and AZD5305. To achieve this, large tumors that were progressing on AZD5305 as a single agent were randomized to receive either AZD5305 (10 mg/kg) as a single agent or a combination of AZD5305 (10 mg/kg) and KSQ-4279 (100 mg/kg). As expected, the tumors in the AZD5305 single-agent arm continued to grow rapidly. In contrast, despite the large tumor size, tumors receiving the combination of AZD5305 and KSQ-4279 regressed over the next 6 weeks of dosing (**Fig. 7B**).

To investigate the activity of KSQ-4279/olaparib combinations in treatment-refractory disease, we performed studies using ovarian orthotopic PDX models generated from patient tumor samples that had relapsed after multiple rounds of chemotherapy and/or PARPi treatment (20). Each of the models tested contained BRCA1 mutations yet were found to be HR-proficient and resistant to PARPi treatment (**Fig. 7C**). In contrast to the relative lack of response to monotherapy treatment, the combination of KSQ-4279 (100 mg/kg) and olaparib (100 mg/kg) once again led to strong antitumor efficacy, including the induction of regressions in the DF68 and DF101 models (**Fig. 7D**).

Discussion

The work presented herein describes the discovery and characterization of the USP1 inhibitor KSQ-4279. CRISPR-Cas9 screening identified *USP1* as an essential target in a subset of ovarian and breast cancer cell lines. Up to 50% of ovarian cancers and 25% of breast cancer samples are associated with defects in the HR pathway, including mutations in *BRCA1* and *BRCA2* (11), and USP1 expression is enriched in HR-defective basal-like breast cancers and BRCA1-mutant ovarian cancers that were resistant to platinum agents (27). To determine whether targeting USP1 in BRCA-mutant and other HR-defective tumors could improve patient outcomes and overcome resistance to PARP inhibitors, we developed KSQ-4279, a potent and selective USP1 inhibitor. In preclinical models, KSQ-4279 was not only active in BRCA-mutant, HR-defective tumor models as a single agent but also synergized with PARP inhibitors when dosed in combination. This combination was also effective in overcoming PARP inhibitor resistance, which is frequently observed in clinical practice.

Mechanism of action studies in BRCA-mutant cells indicated that sensitivity to KSQ-4279 is primarily due to dysregulation of the ubiquitination of PCNA rather than FANCD2. PCNA is monoubiquitinated in response to fork stalling at sites of damaged DNA which can trigger TLS by recruiting specialized, low-fidelity DNA polymerases to proceed past the DNA lesion. USP1 deubiquitinates PCNA, enabling the replication fork to resume its high-fidelity replication. KSQ-4279-mediated inhibition of USP1 and resulting accumulation of Ub-PCNA would therefore be predicted to lead to excessive TLS replication with low-fidelity DNA polymerases. However, it is not clear what the consequences of this would be and if it would explain the specific sensitivity of BRCA-mutant cells. TLS has been associated with ssDNA gap suppression in BRCA-mutant cells (52, 53) and our findings indicate that, conversely, USP1 inhibition leads to an accumulation of ssDNA gaps (**Fig. 5C**). The absence of TLS

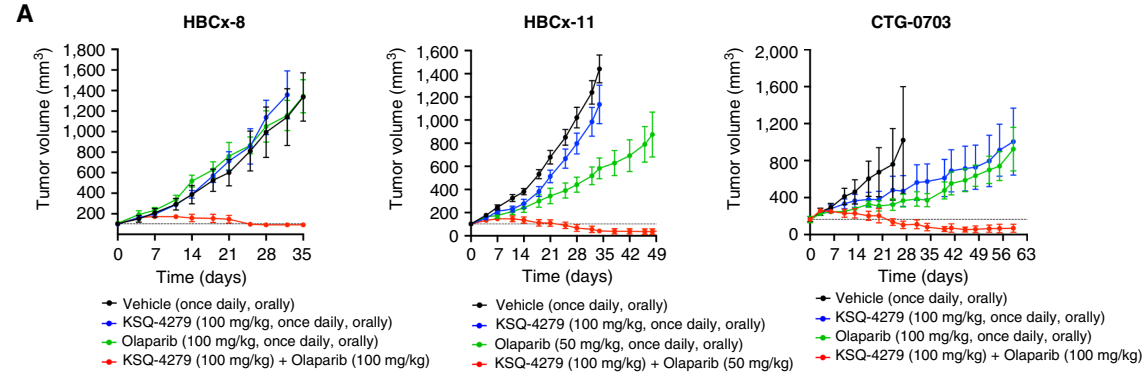

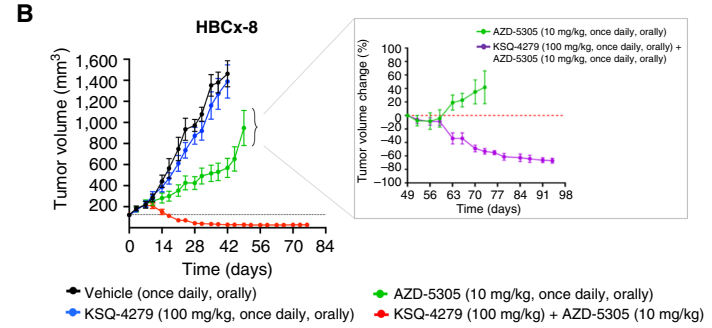

C

Model	Source	# prior lines of chemo	Prior platinum	BRCA status	Additional mutations	RAD51 foci assay
DF-59	Ascities	7	Yes	BRCA1 5385insC	NA	HR proficient
DF-68	Ascities	5	Yes	BRCA1 Q563X	TP53, BRCA1and PTEN (copy loss)	HR proficient
DF-86	Ascities	6	Yes	BRCA1 del exons 21-24	TP53, BRCA1and APC	HR proficient
DF-101	Pleural fluid	2	Yes	BRCA1 del 187delAG	TP53, BRCA1, NBN and PTEN (copy loss)	HR proficient

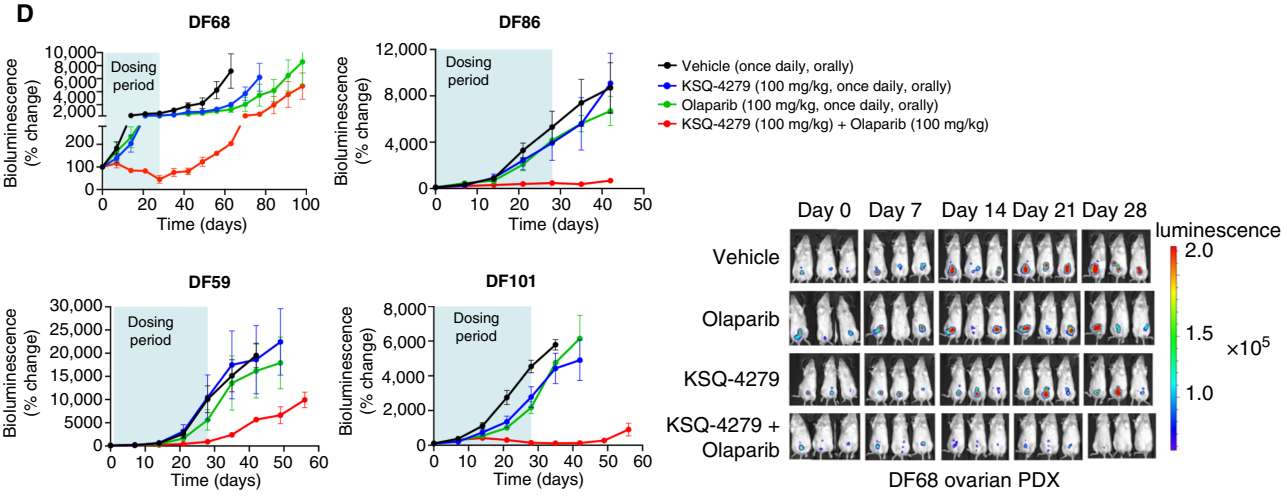

Figure 7.

A, Tumor growth curves for the PDX models HBCx-8, HBCx-11, and CTG-0703, treated once daily via oral gavage, with vehicle control, KSQ-4279, olaparib or the combination of KSQ-4279 and olaparib at the indicated doses. Mice (n = 3–10/group) were randomized, and treatment administered once the mean tumor volume reached approximately 200 mm^3, denoted as day 0. The horizontal dotted black line represents the mean tumor volume in the combination-treated group on day 0, prior to treatment initiation. **B,** Tumor growth curves for the HBCx-8 model, treated with KSQ-4279, AZD5305, or the combination of KSQ-4279 and AZD5305 at the indicated doses. Around day 50, tumors that were progressing on single-agent treatment with AZD5305 were randomized and allocated into either receiving AZD5305 alone or a combination of KSQ-4279 and AZD5305. **C,** Clinical history and mutational profiles of the four PARPi-resistant BRCA1-mutant orthotopic ovarian cancer ascites models evaluated in the study. **D,** Following initiation of dosing, each orthotopic model was monitored by bioluminescence, and percent of change was plotted graphically, with representative images of luciferase bioluminescence signal for the ovarian PDX DF68 shown. Each orthotopic model was treated once daily for 28 days via oral gavage with vehicle control, 100 mg/kg olaparib, 100 mg/kg KSQ-4279, or the combination of 100 mg/kg olaparib and 100 mg/kg KSQ-4279. Mice were randomized, and treatment was administered 7 days after transfer of luciferase-tagged human ovarian cancer cells, denoted as day 0.

polymerases scoring as significant factors influencing the sensitivity of cells to KSQ-4279 in the CRISPR screen also suggests TLS activity may not be a major driver of sensitivity (**Fig. 6A**). Alternatively, the sensitivity of BRCA-mutant cells to KSQ-4279 may relate to the observation that USP1 can become trapped at sites of active DNA synthesis if the autocleavage of USP1 is impaired (54). Because the catalytic activity of USP1 is required for its own autocleavage, it is conceivable that KSQ-4279 prevents the autocleavage of USP1 leading

to USP1 remaining trapped within the replication fork. Because BRCA-mutant cells are known to have inherently unstable replication forks and depend on USP1 to maintain fork stability (27), further fork destabilization as a result of USP1-trapping may be involved in the sensitivity of BRCA-mutant cells to KSQ-4279.

The observation that the sensitivity of BRCA-mutant cells to KSQ-4279 is enhanced upon CRISPR-mediated inactivation of PARP1, and other members of the base-excision pathway, led to further studies that revealed a striking synergy between KSQ-4279 and PARP inhibitors such as olaparib. The specific mechanism behind the critical interdependence of these two pathways remains unknown; however, different scenarios may be at play. For example, ssDNA gap formation and replication fork instability induced by KSQ-4279 may increase the workload of ssDNA repair pathways, which leads to increased PARP trapping and, in turn, greater cytotoxicity of BRCA-mutant cells. Alternatively, cotreatment of USP1 and PARP1 inhibitors may simply overwhelm the ability of HR-defective cells to tolerate the ssDNA gap formation and replication fork dysregulation independently induced by both agents. Another possibility may relate to the importance of PCNA for long-patch BER, which may be dysregulated by the influence of KSQ-4279 on PCNA ubiquitination and exacerbate the impact of PARP inhibitors.

Despite the clinical success of PARP inhibitors, resistance invariably develops and remains a high unmet clinical need. The development of KSQ-4279 is an important therapeutic option for these patients. To determine if the efficacious exposures of KSQ-4279 observed in the mouse xenograft studies would be achievable in humans, a physiologically based pharmacokinetic modeling approach was used. This calculation incorporated the minimum circulating levels of KSQ-4279 required for efficacy, the relationship between the mouse PK and PD response (Ub-PCNA levels), and the cross-species PK profiles corrected for plasma protein binding. This analysis estimated that once daily dosing of KSQ-4279 in the range of 300 to 480 mg would achieve plasma levels similar to those that achieved efficacy in the mouse models.

Results for the first-in-human trial of KSQ-4279 were recently presented (55). KSQ-4279 was dosed up to 1,250 mg once a day and was reported to have an acceptable safety profile with the most common treatment-emergent adverse events being anemia and increased creatinine. Paired biopsies from patients before and after treatment with KSQ-4279 confirmed the inhibition of USP1 as the mechanism of action with evidence of clinical activity seen in a patient with fallopian tube cancer.

Collectively, our findings indicate that USP1 inhibition with KSQ-4279 in combination with PARP inhibitors presents a broad therapeutic opportunity for patients with BRCA-mutant/HR-deficient cancers that are resistant or refractory to PARP inhibitor therapy, including the new generation of PARP1-selective inhibitors. The findings in our study position KSQ-4279 and the targeting of USP1 as a promising new approach to address the high unmet clinical need for new therapies to treat BRCA-mutant/HR-defective tumors and is currently in clinical testing.

Authors' Disclosures

E. Krall reports personal fees from Merck Sharp and Dohme LLC outside the submitted work, as well as a patent 11485736 issued. E. Chipumuro reports other support from KSQ Therapeutics outside the submitted work. K. Sinkevicius reports employment with KSQ Therapeutics and receiving KSQ Therapeutics stock options. P.C. Gokhale reports grants from KSQ Therapeutics, Inc. during the conduct of the study, as well as grants from Kymera Therapeutics, Pfizer Inc., Treeline Biosciences, and Arvinas outside the submitted work. U.A. Matulonis reports personal fees from Tango Therapeutics, ProfoundBio, NextCure, Eisai, ImmunoGen, AbbVie, Alkermes, Novartis, and GSK outside the submitted work. J.F. Liu reports personal fees from AstraZeneca, Bristol Myers Squibb, Clovis Oncology, Daiichi Sankyo, Eisai, Genentech/Roche, GlaxoSmithKline, Regeneron Therapeutics, and Zentalis Pharmaceuticals outside the submitted work. M. Schlabach reports a patent for US 2021/0115049 A1 pending. F. Stegmeier reports full-time employment with KSQ Therapeutics during the time of this work, as well as being on the Board of Directors and ownership of stocks in KSQ Therapeutics. A.A. Wylie reports personal fees from KSQ Therapeutics outside the submitted work, as well as a patent for WO2021163530A1 issued, WO20230203046A1 issued, and WO2023147311A1 issued. J. Brenneman, J.J. Ali, S. Shenker, M. McGuire, P. Grasberger, Y. Mishina, E. Krall, J. Hixon, E. Chipumuro, K. Sinkevicius, A. Olaharski, H. Liu, J. Wilt, M. Schlabach, and F. Stegmeier conducted this research while employed by KSQ Therapeutics. No disclosures were reported by the other authors.

Authors' Contributions

L. Cadzow: Conceptualization, supervision, writing–review and editing. **J. Brenneman:** Conceptualization, supervision. **E. Tobin:** Conceptualization, supervision, writing–review and editing. **P. Sullivan:** Supervision, investigation. **S. Nayak:** Conceptualization, investigation, writing–review and editing. **J.A. Ali:** Conceptualization, supervision, writing–original draft. **S. Shenker:** Conceptualization, data curation, software. **J. Griffith:** Conceptualization, formal analysis, supervision. **M. McGuire:** Investigation. **P. Grasberger:** Investigation. **Y. Mishina:** Investigation. **M. Murray:** Investigation. **A.E. Dodson:** Conceptualization, software, investigation. **H. Gannon:** Supervision. **E. Krall:** Conceptualization, supervision. **J. Hixon:** Conceptualization, supervision. **E. Chipumuro:** Supervision, investigation. **K. Sinkevicius:** Conceptualization, supervision. **P.C. Gokhale:** Conceptualization, supervision. **S. Ganapathy:** Investigation. **U.A. Matulonis:** supervision. **J.F. Liu:** Conceptualization, supervision. **A. Olaharski:** Conceptualization, supervision. **D. Sangurdekar:** Conceptualization, supervision. **H. Liu:** Conceptualization, supervision. **J. Wilt:** Conceptualization, supervision. **M. Schlabach:** Conceptualization, supervision. **F. Stegmeier:** Conceptualization, supervision, writing–review and editing. **A.A. Wylie:** Conceptualization, supervision, writing–original draft.

Acknowledgments

The authors would like to thank the following contract research organizations for supporting this work: Biortus, ChemPartner, Crown Bioscience, intoDNA, Pharmaron, Ubiquigent, and Xentech. All work was sponsored by KSQ Therapeutics.

Note

Supplementary data for this article are available at Cancer Research Online (http://cancerres.aacrjournals.org/).

Received January 25, 2024; revised May 24, 2024; accepted August 20, 2024; published first August 26, 2024.

References

1. Negrini S, Gorgoulis VG, Halazonetis TD. Genomic instability-an evolving hallmark of cancer. Nat Rev Mol Cell Biol 2010;11:220–8.
2. Hanahan D, Weinberg RA. Hallmarks of cancer: the next generation. Cell 2011;144:646–74.
3. Shaheen FS, Znojek P, Fisher A, Webster M, Plummer R, Gaughan L, et al. Targeting the dna double strand break repair machinery in prostate cancer. PLoS One 2011;6:e20311.
4. Gudmundsdottir K, Ashworth A. The roles of BRCA1 and BRCA2 and associated proteins in the maintenance of genomic stability. Oncogene 2006;25:5864–74.
5. Lomonosov M, Anand S, Sangrithi M, Davies R, Venkitaraman AR. Stabilization of stalled DNA replication forks by the BRCA2 breast cancer susceptibility protein. Genes Dev 2003;17:3017–22.
6. Schlacher K, Wu H, Jasin M. A distinct replication fork protection pathway connects Fanconi anemia tumor suppressors to RAD51-BRCA1/2. Cancer Cell 2012;22:106–16.

7. Schlacher K, Christ N, Siaud N, Egashira A, Wu H, Jasin M. Double-strand break repair-independent role for BRCA2 in blocking stalled replication fork degradation by MRE11. Cell 2011;145:529–42.
8. Lord CJ, Ashworth A. PARP inhibitors: synthetic lethality in the clinic. Science 2017;355:1152–8.
9. Chan EM, Shibue T, McFarland JM, Gaeta B, Ghandi M, Dumont N, et al. WRN helicase is a synthetic lethal target in microsatellite unstable cancers. Nature 2019;568:551–6.
10. Ali RMM, McIntosh SA, Savage KI. Homologous recombination deficiency in breast cancer: implications for risk, cancer development, and therapy. Genes Chromosomes Cancer 2021;60:358–72.
11. Nguyen L, Martens JWM, Van Hoeck A, Cuppen E. Pan-cancer landscape of homologous recombination deficiency. Nat Commun 2020;11:1–12.
12. Konstantinopoulos PA, Ceccaldi R, Shapiro GI, D'Andrea AD. Homologous recombination deficiency: exploiting the fundamental vulnerability of ovarian cancer. Cancer Discov 2015;5:1137–54.
13. Ceccaldi R, Sarangi P, D'Andrea AD. The Fanconi anaemia pathway: new players and new functions. Nat Rev Mol Cell Biol 2016;17:337–49.
14. García-Santisteban I, Peters GJ, Giovannetti E, Rodríguez JA. USP1 deubiquitinase: cellular functions, regulatory mechanisms and emerging potential as target in cancer therapy. Mol Cancer 2013;12:91.
15. Wang T, Wei JJ, Sabatini DM, Lander ES. Genetic screens in human cells using the CRISPR-Cas9 system. Science 2014;343:80–4.
16. Villamil MA, Chen J, Liang Q, Zhuang Z. A noncanonical cysteine protease USP1 is activated through active site modulation by USP1-associated factor 1. Biochemistry 2012;51:2829–39.
17. Villamil MA, Liang Q, Chen J, Choi YS, Hou S, Lee KH, et al. Serine phosphorylation is critical for the activation of ubiquitin-specific protease 1 and its interaction with WD40-repeat protein UAF1. Biochemistry 2012;51:9112–23.
18. Mistry H, Hsieh G, Buhrlage SJ, Huang M, Park E, Cuny GD, et al. Small-molecule inhibitors of USP1 target ID1 degradation in leukemic cells. Mol Cancer Ther 2013;12:2651–62.
19. Hassiepen U, Eidhoff U, Meder G, Bulber J-F, Hein A, Bodendorf U, et al. A sensitive fluorescence intensity assay for deubiquitinating proteases using ubiquitin-rhodamine110-glycine as substrate. Anal Biochem 2007;371:201–7.
20. Liu JF, Palakurthi S, Zeng Q, Zhou S, Ivanova E, Huang W, et al. Establishment of patient-derived tumor xenograft models of epithelial ovarian cancer for preclinical evaluation of novel therapeutics. Clin Cancer Res 2017;23:1263–73.
21. Nijman SMB, Huang TT, Dirac AMG, Brummelkamp TR, Kerkhoven RM, D'Andrea AD, et al. The deubiquitinating enzyme USP1 regulates the Fanconi anemia pathway. Mol Cell 2005;17:331–9.
22. Huang TT, Nijman SMB, Mirchandani KD, Galardy PJ, Cohn MA, Haas W, et al. Regulation of monoubiquitinated PCNA by DUB autocleavage. Nat Cell Biol 2006;8:339–47.
23. Cohn MA, Kowal P, Yang K, Haas W, Huang TT, Gygi SP, et al. A UAF1-containing multisubunit protein complex regulates the Fanconi anemia pathway. Mol Cell 2007;28:786–97.
24. Lord CJ, Ashworth A. BRCAness revisited. Nat Rev Cancer 2016;16:110–20.
25. Bianchini G, Balko JM, Mayer IA, Sanders ME, Gianni L. Triple-negative breast cancer: challenges and opportunities of a heterogeneous disease. Nat Rev Clin Oncol 2016;13:674–90.
26. Takaya H, Nakai H, Takamatsu S, Mandai M, Matsumura N. Homologous recombination deficiency status-based classification of high-grade serous ovarian carcinoma. Sci Rep 2020;10:2757.
27. Lim KS, Li H, Roberts EA, Gaudiano EF, Clairmont C, Sambel LA, et al. USP1 is required for replication fork protection in BRCA1-deficient tumors. Mol Cell 2018;72:925–41.e4.
28. Manchana T, Phoolcharoen N, Tantbirojn P. BRCA mutation in high grade epithelial ovarian cancers. Gynecol Oncol Rep 2019;29:102–5.
29. Pogoda K, Niwińska A, Sarnowska E, Nowakowska D, Jagiełło-Gruszfeld A, Siedlecki J, et al. Effects of BRCA germline mutations on triple-negative breast cancer prognosis. J Oncol 2020;2020:854564.
30. Harrigan JA, Jacq X, Martin NM, Jackson SP. Deubiquitylating enzymes and drug discovery: emerging opportunities. Nat Rev Drug Discov 2018;17:57–78.
31. Mah L-J, El-Osta A, Karagiannis TC. gammaH2AX: a sensitive molecular marker of DNA damage and repair. Leukemia 2010;24:679–86.
32. Al-kaabi MM, Alshareeda AT, Jerjees DA, Muftah AA, Green AR, Alsubhi NH, et al. Checkpoint kinase1 (CHK1) is an important biomarker in breast cancer having a role in chemotherapy response. Br J Cancer 2015;112:901–11.
33. Porter AG, Jänicke RU. Emerging roles of caspase-3 in apoptosis. Cell Death Differ 1999;6:99–104.
34. Li M, Larsen L, Hedglin M. Rad6/Rad18 competes with DNA polymerases η and δ for PCNA encircling DNA. Biochemistry 2020;59:407–16.
35. Kanao R, Masutani C. Regulation of DNA damage tolerance in mammalian cells by post-translational modifications of PCNA. Mutat Res 2017;803–805:82–8.
36. Simoneau A, Engel JL, Bandi M, Lazarides K, Liu S, Meier SR, et al. Ubiquitinated PCNA drives USP1 synthetic lethality in cancer. Mol Cancer Ther 2023;22:215–26.
37. Maya-Mendoza A, Moudry P, Merchut-Maya JM, Lee M, Strauss R, Bartek J. High speed of fork progression induces DNA replication stress and genomic instability. Nature 2018;559:279–84.
38. Cong K, Peng M, Kousholt AN, Lee WTC, Lee S, Nayak S, et al. Replication gaps are a key determinant of PARP inhibitor synthetic lethality with BRCA deficiency. Mol Cell 2021;81:3128–44.e7.
39. Quinet A, Carvajal-Maldonado D, Lemacon D, Vindigni A. DNA fiber analysis: mind the gap. Methods Enzymol 2017;591:55–82.
40. Kuzminov A. Single-strand interruptions in replicating chromosomes cause double-strand breaks. Proc Natl Acad Sci U S A 2001;98:8241–6.
41. Ceccaldi R, Rondinelli B, D'Andrea AD. Repair pathway choices and consequences at the double-strand break. Trends Cell Biol 2016;26:52–64.
42. Ray Chaudhuri A, Nussenzweig A. The multifaceted roles of PARP1 in DNA repair and chromatin remodelling. Nat Rev Mol Cell Biol 2017;18:610–21.
43. Chen R, Wold MS. Replication protein A: single-stranded DNA's first responder: dynamic DNA-interactions allow replication protein A to direct single-strand DNA intermediates into different pathways for synthesis or repair. Bioessays 2014;36:1156–61.
44. Zhao F, Kim W, Kloeber JA, Lou Z. DNA end resection and its role in DNA replication and DSB repair choice in mammalian cells. Exp Mol Med 2020;52:1705–14.
45. Choe KN, Moldovan G-L. Forging ahead through darkness: PCNA, still the principal conductor at the replication fork. Mol Cell 2017;65:380–92.
46. Hoege C, Pfander B, Moldovan G-L, Pyrowolakis G, Jentsch S. RAD6-dependent DNA repair is linked to modification of PCNA by ubiquitin and SUMO. Nature 2002;419:135–41.
47. Gallina I, Hendriks IA, Hoffmann S, Larsen NB, Johansen J, Colding-Christensen CS, et al. The ubiquitin ligase RFWD3 is required for translesion DNA synthesis. Mol Cell 2021;81:442–58.e9.
48. Kim D, Nam HJ. PARP inhibitors: clinical limitations and recent attempts to overcome them. Int J Mol Sci 2022;23:8412.
49. Illuzzi G, Staniszewska AD, Gill SJ, Pike A, McWilliams L, Critchlow SE, et al. Preclinical characterization of AZD5305, a next-generation, highly selective PARP1 inhibitor and trapper. Clin Cancer Res 2022;28:4724–36.
50. Lee EK, Matulonis UA. PARP inhibitor resistance mechanisms and implications for post-progression combination therapies. Cancers (Basel) 2020;12:2054.
51. Castroviejo-Bermejo M, Cruz C, Llop-Guevara A, Gutiérrez-Enríquez S, Ducy M, Ibrahim YH, et al. A RAD51 assay feasible in routine tumor samples calls PARP inhibitor response beyond BRCA mutation. EMBO Mol Med 2018;10:e9172.
52. Cong K, Cantor SB. Exploiting replication gaps for cancer therapy. Mol Cell 2022;82:2363–9.
53. Nayak S, Calvo JA, Cantor SB. Targeting translesion synthesis (TLS) to expose replication gaps, a unique cancer vulnerability. Expert Opin Ther Targets 2021;25:27–36.
54. Coleman KE, Yin Y, Lui SKL, Keegan S, Fenyo D, Smith DJ, et al. USP1-trapping lesions as a source of DNA replication stress and genomic instability. Nat Commun 2022;13:1740.
55. Yap TA, Lakhani NJ, Patnaik A, Lee EK, Gutierrez M, Moore KN, et al. First-in-human phase I trial of the oral first-in-class ubiquitin specific peptidase 1 (USP1) inhibitor KSQ-4279 (KSQi), given as single agent (SA) and in combination with olaparib (OLA) or carboplatin (CARBO) in patients (pts) with advanced solid tumors, enriched for deleterious homologous recombination repair (HRR) mutations. J Clin Oncol 2024;42:3005.